physica status solidi a
www.pss-a.com

Lattice-Mismatched Epitaxy of InAs on (111)A-Oriented Substrate: Metamorphic Layer Growth and Self-Assembly of Quantum Dots

Takaaki Mano, Akihiro Ohtake, and Takashi Kuroda*

In this article, recent developments in the lattice-mismatched epitaxy of InAs on (111)A-oriented substrates and related research topics, in which the presence or absence of the misfit dislocations is controlled via prescribed growth sequences, are reviewed. When InAs is grown on GaAs (111)A substrates, a unique lattice-relaxation mechanism occurs. A misfit dislocation network is formed at the initial stage of InAs growth, that is followed by the layer-by-layer growth of relaxed InAs films. The InAs/GaAs (111)A heterostructure is being applied in infrared photodetectors which have a new operating principle that employs the high-density dislocations at the interface. The InAs/GaAs (111)A heterostructure is also useful for the growth of InGaAs layers: a nearly lattice-relaxed InGaAs containing different concentrations of indium can be formed by inserting a thin-InAs layer between the InGaAs and GaAs. These InGaAs layers can be used as virtual substrates with a desired lattice constant for a range of devices. In addition to the formation of lattice-relaxed structures, dislocation-free InAs quantum dots (QDs) can be formed on InP (111)A substrates by applying droplet epitaxy. The C_{3v} symmetry of the (111)A surface makes it possible to form symmetric InAs QDs that emit entangled photon pairs at telecommunication wavelengths.

1. Introduction

Heteroepitaxial growth of III–V semiconductors on lattice-mismatched substrates has been investigated for many years, hoping to open new possibilities for band-structure engineering and novel devices.[1,2] During epitaxial growth, it is critically important to manage lattice mismatching. When the grown layer is thinner than the critical thickness for dislocation formation, a pseudomorphic layer is formed, in which the layer is strained and dislocation free.[3] The strained-layer structures are suitable for optical devices such as light-emitting diodes. By tuning the lattice mismatch, it is also possible to form 3D islands or quantum dots (QDs) in the Stranski–Krastanov (SK) mode.[4–6] A typical example is InAs/GaAs: after the growth of a few monolayer (ML)-thick 2D layers (often called wetting layers), 3D InAs islands are formed. The islands are strained and dislocation free, and application to several optical devices has been demonstrated that exploits their highly luminescent properties. In the past two decades, InAs QD growth on GaAs (100) in SK mode has been an intensively studied research topic, anticipating its application to high-performance lasers and quantum light emitters.[7,8]

While strained layers or islands without dislocations are useful as active layers of optical devices, there has also been interest in growing lattice-relaxed heteroepitaxial layers (metamorphic layers) by deliberately introducing misfit dislocations.[9–12] These metamorphic layers can act as virtual substrates with lattice constants set at desired values.[13–15] Narrow-gap semiconductor substrates, such as InAs, GaSb, or InSb, tend to be more expensive than those of versatile GaAs or InP substrates. To reduce the cost of devices such as infrared photodetectors and magnetic sensors, many groups have been investigating how to grow metamorphic narrow-gap semiconductors on GaAs or InP substrates.[16,17] Heteroepitaxial growth on (111)A substrates is a very interesting system for forming metamorphic layers.[18,19] It has been reported that InAs film grows in layer-by-layer mode on GaAs (111)A substrates from the beginning to the end of the growth process.[18,20–23] The layer-by-layer growth is accompanied by the formation of a misfit dislocation network at the InAs/GaAs interface.[21,23] This growth mechanism is entirely different to that of SK growth on (100) substrate.[4] We have recently revisited this InAs growth on lattice-mismatched (111)A substrates and found several challenges and new possibilities.[23–26]

This review will focus on InAs growth on lattice-mismatched GaAs and InP (111)A substrates and related topics. After providing an overview of the basic characteristics of the (111)A surfaces, we will summarize recent progress on the metamorphic growth of InAs on GaAs (111)A and its application to the infrared photodetectors. We will then describe the InAs QDs formation of (111)A substrates, for which SK growth cannot be used.

T. Mano, A. Ohtake, T. Kuroda
Research Center for Electronic and Optical Materials
National Institute for Materials Science
1-2-1 Sengen, Tsukuba, Ibaraki 305-0047, Japan
E-mail: mano.takaaki@nims.go.jp

The ORCID identification number(s) for the author(s) of this article can be found under https://doi.org/10.1002/pssa.202300767.

DOI: 10.1002/pssa.202300767

2. Basic Characteristic of (111)A Substrates

The surfaces of III–V compound semiconductors exhibit a variety of surface reconstructions depending on their surface orientations, temperature, background pressure of V-group element atoms, and so on. For the growth of high-quality layers, it is important to understand and control the surface structures. In this section, we briefly overview the surface reconstructions of (111)A surfaces (mainly well-studied GaAs surfaces) and typical growth conditions on surfaces that usually require more precise tuning than those on standard (001) surfaces.

2.1. Surface Reconstruction of GaAs (111)A

The surface structures of GaAs (001) change from As-rich c(4 × 4)β to Ga-rich (4×6) through the c(4 × 4)α, (2 × 4), (6 × 6), and c(8 × 2) phases, which are influenced by temperature and background As flux.[27] In contrast, a polar GaAs (111)A surface normally shows only a Ga-rich (2 × 2) reconstructed surface.[28–31] Note that As-rich (2 × 2) reconstruction can also (exceptionally) occur when a (111)A surface covered with amorphous As is thermally annealed.[32] The reason that only the (2 × 2) reconstruction appears is not fully understood. It is likely related to the low sticking coefficient of As molecules to the (111)A surface.[33] The III-antimonide (111)A surfaces exhibit not only (2 × 2) but also other reconstructions,[34] which can be attributed to the higher sticking coefficient of Sb molecules to the surfaces than that of As. **Figure 1**a shows filled-state scanning tunneling microscopy (STM) images of GaAs (111)A-(2 × 2) surfaces.[31] Tong et al. first proposed the Ga-vacancy buckling structure model for this reconstructed surface,[28] as seen in Figure 1b, which has since been confirmed by STM,[30,31] reflection high-energy electron diffraction (RHEED),[31] and first-principles calculations.[31] At the top layer, one fourth of the Ga atoms are missing. The (111)A surface of InAs, InAlAs, and InP also shows the (2 × 2) reconstruction with the same atomic structure, while other reconstructions can be observed in some cases.[35,36]

2.2. Typical Growth Condition on (111)A

The standard conditions for growth on (111)A surfaces in molecular beam epitaxy (MBE) is different from those on (001) surfaces. Because of the low V-group element atom sticking coefficient on the surface, it is necessary to use the high V/III ratios and/or low growth temperatures.[33,37] Here, we describe GaAs growth on GaAs (111)A as an example. Typically, growth temperatures are set at below 550 °C for the growth of GaAs on GaAs (111)A, while temperatures above 580 °C are normally used for growth on GaAs (001).[18,33,38] If the growth parameters deviate from the optimized condition, stacking faults (SFs), and/or hillock structures begin to form,[39] as seen in **Figure 2**. In the lattice-matched systems of AlGaAs on GaAs (111)A, InAlAs on InP(111)A, and InGaAs on InP (111)A, the optimized parameter windows for the growth of high-quality layer are narrower than that for GaAs homoepitaxy.[40,41] As seen in **Figure 3** and **4**, surface morphology is highly sensitive to growth

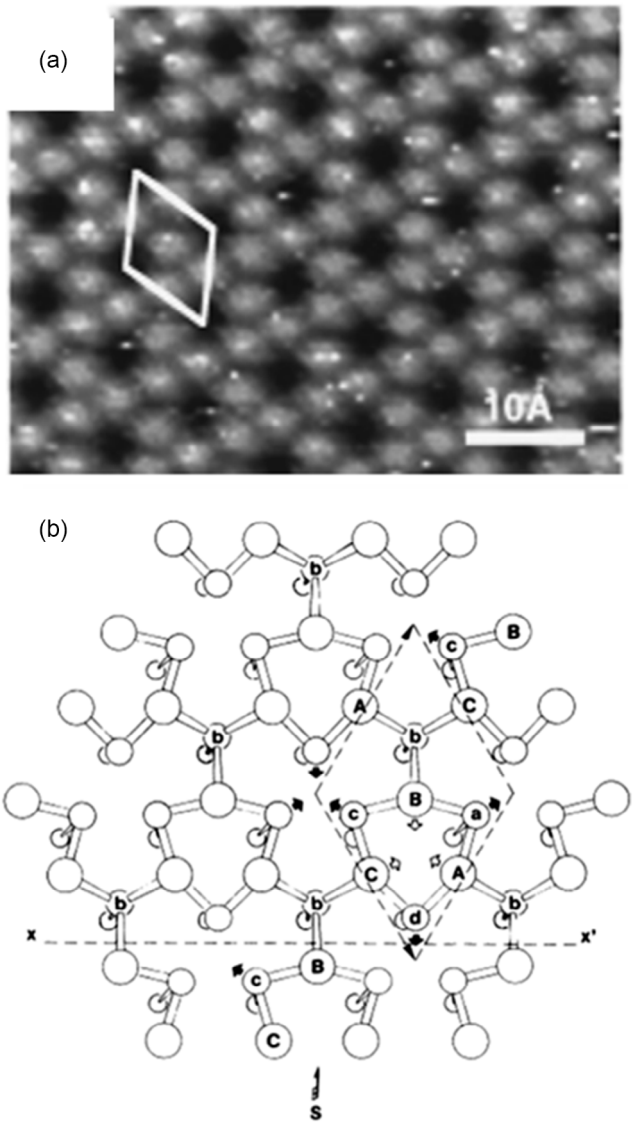

Figure 1. a) Filled-state scanning tunneling microscopy (STM) images of the GaAs (111)A-(2 × 2) surface. Image dimension is 6.5 × 5.3 nm. The STM observation was performed at room temperature in the constant-current mode with a tunneling current of 0.5 nA and a negative sample voltage. The surface was prepared by growth of GaAs at 400 °C on GaAs (111)A substrate with an As_4/Ga flux ratio of ≈150. After subsequent thermal annealing, the sample was transferred to an STM chamber. b) Top view of the vacancy-buckling structure model. The structural determination was done by analysis of low-energy electron diffraction (LEED) intensity-voltage data using a fully convergent multiple-scattering method. Reproduced with permission.[28,31] (a) Copyright 2001 and (b) Copyright 1984, The American Physical Society.

conditions. Careful optimization of the growth parameters such as growth temperature and V/III ratio is required for the growth of smooth layers.

To prevent the need for precise control of growth conditions, several alternative methods have been proposed. By using misoriented substrates (2° miscut), smooth surfaces can be easily obtained, even at high growth rates.[42,43] More recently,

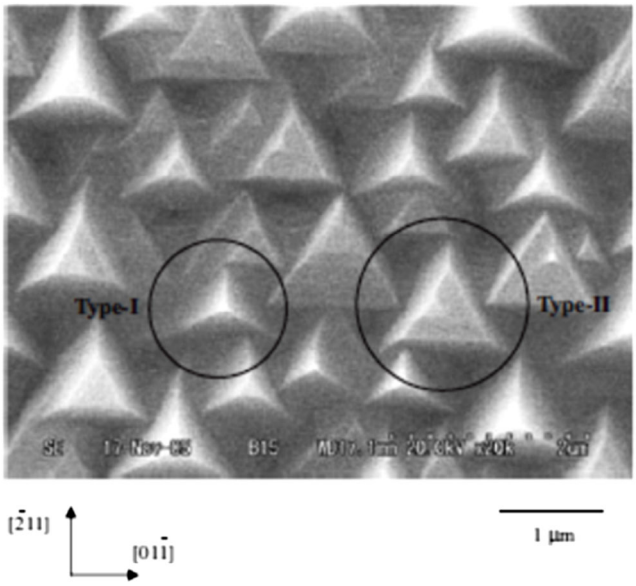

Figure 2. Scanning electron microscopy image of the surface of GaAs grown on GaAs (111)A substrate. The GaAs layer was grown by migration-enhanced epitaxy at 590 °C with an As_4 beam equivalent pressure of 1.0×10^{-5} Torr. Reproduced with permission.[39] Copyright 2007, IOP Publishing.

surfactant-enhanced epitaxy has also been reported. Using bismuth, surface defects/hillocks are effectively eliminated and atomically smooth surfaces are obtained.[44]

3. Metamorphic Growth on InAs

3.1. InAs Growth on GaAs(111)A Substrates

Figure 5a shows the evolution of the RHEED pattern during the growth of InAs on GaAs (111)A.[18] Streak patterns are maintained from the beginning to even after 30 ML InAs growth, suggesting continuous layer-by-layer growth. This growth feature on (111)A is entirely different from the growth of InAs on GaAs (001).[6,18] On GaAs (001), streak patterns are also maintained at the beginning of the growth process, but these change into a spotty pattern when the thickness of InAs exceeds 1.5–1.7 ML, indicating the growth of a 2D layer (wetting layer) and the subsequent formation of 3D islands. This form of growth is called the SK mode. The 3D InAs islands are dislocation free and are elastically strained, and can be used as QDs. By further increasing the amount of InAs, misfit dislocations are formed that gradually relax the accumulated strain.[9] Figure 5b shows atomic force microscopy (AFM) images after the growth of 10 ML InAs on GaAs (001) and (111)A.[18] It is clear that a smooth surface is formed on (111)A (consists of a step-and-terrace structure[21,23]), whereas high-density 3D islands are visible on (001). We have confirmed that a smooth surface is maintained even after the growth of 300 nm InAs on GaAs (111)A in our previous paper.[26]

The origin of the layer-by-layer growth mode on the (111)A surface is closely related to the formation of a misfit dislocation

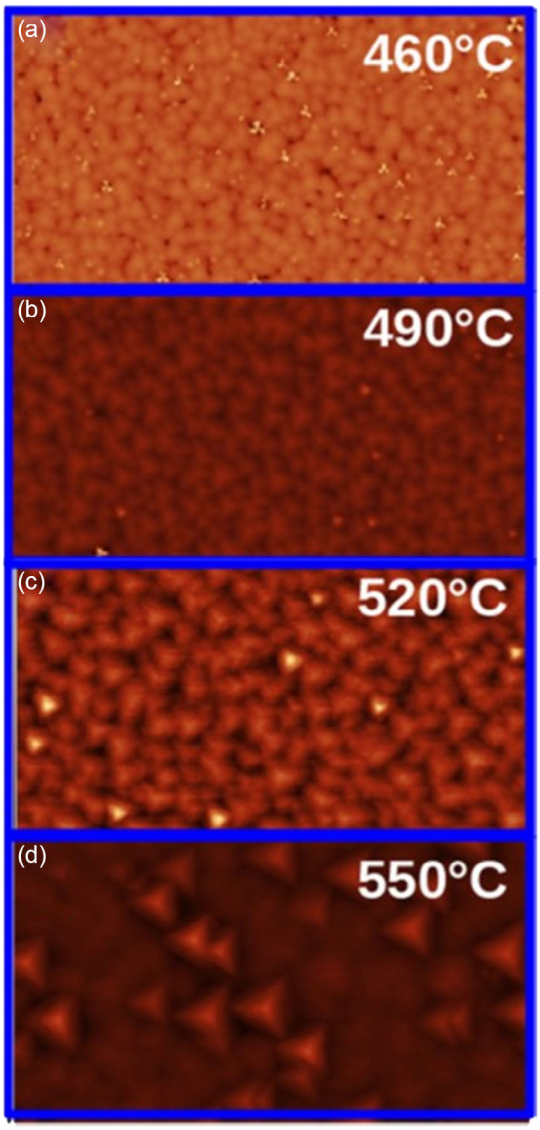

Figure 3. Atomic force microscopy (AFM) images ($4 \times 8\ \mu m^2$) of $Al_{0.30}Ga_{0.70}As$ grown on GaAs (111)A (growth temperature dependence). The 100 nm AlGaAs layers were grown with a group III flux of $6 \times 10^{14}\ s^{-1}\ cm^{-2}$ and a V/III ratio of 75. The growth temperatures (460–550 °C) are indicated in the images. Reproduced with permission.[41] Copyright 2017, The American Physical Society.

network at the InAs–GaAs interface.[21] In STM images made after growing 5 ML InAs, the formation of a dislocation network is clearly visible (**Figure 6**a). The network is not a simple hexagonal structure: partial dislocations form at the interface in addition to the perfect dislocations. A possible structural model of the dislocation network has also been proposed (Figure 6b), in which both the dislocations and SFs are buried at the interface.

The change in the in-plane lattice constant during InAs growth provides more detailed information on the formation of dislocation networks at the initial stage of growth. **Figure 7** shows the evolution of in-plane lattice constants during the

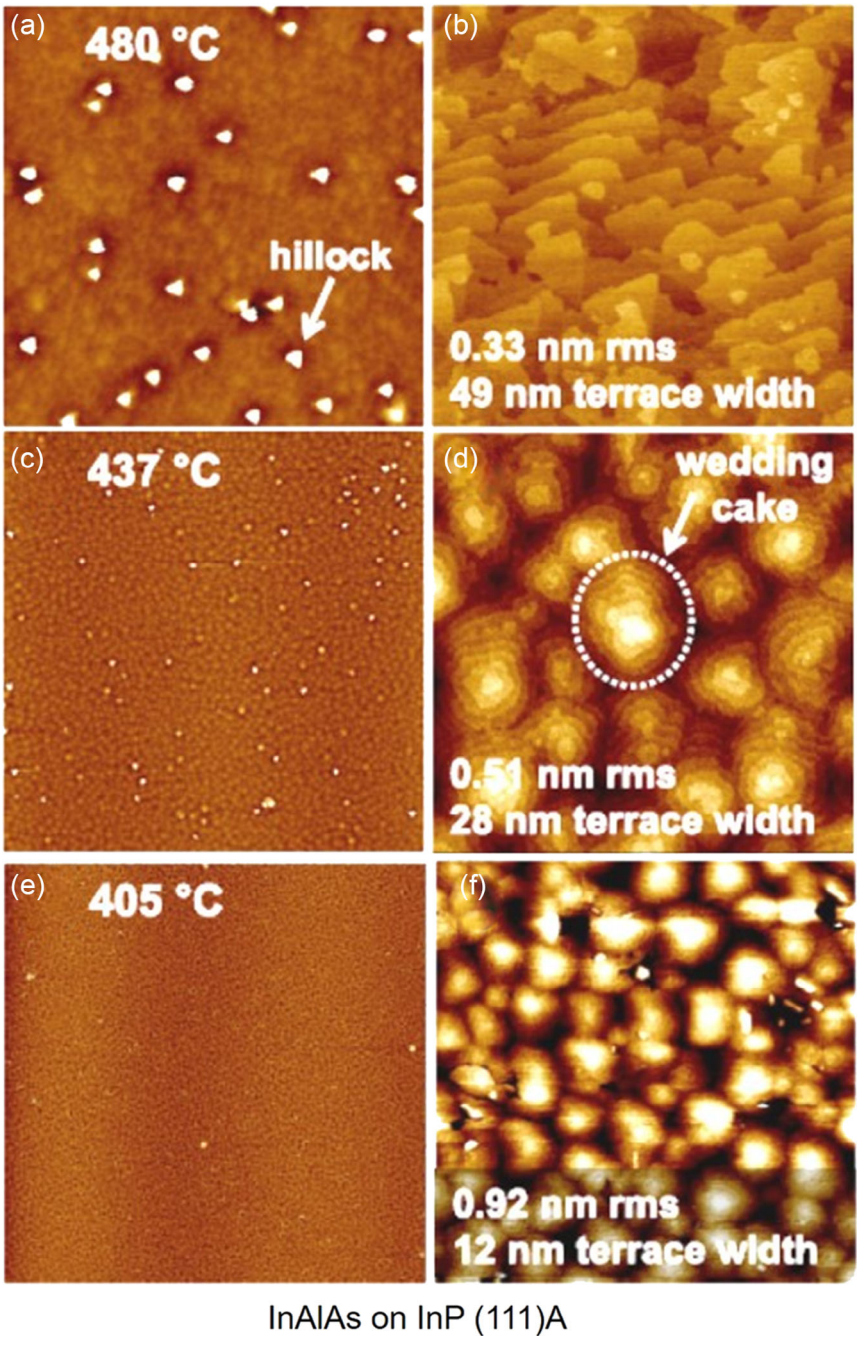

Figure 4. AFM images of $In_{0.52}Al_{0.48}As$ on InP (111)A (growth temperature dependence). The growth temperatures were at a,b) 480 °C, c,d) 437 °C, and e, f) 405 °C. The image sizes are a,c,e) 15 × 15 μm^2 and b,d,f) 1 × 1 μm^2, respectively. The InAlAs layers were grown with a V/III ratio of 230 and a growth rate of 0.17 μm h^{-1}. Reproduced under the terms of the CC-BY license.[40] Copyright 2017, AIP publishing.

growth of InAs.[22] The in-plane lattice constant starts to change when the InAs thickness exceeds 1.5 ML, suggesting that the dislocations begin to form at the interface of InAs and GaAs while the second InAs layer is growing. The relaxation proceeds gradually during growth of 1.5–5 ML InAs, with the lattice constant changing more slowly during the further growth of InAs. Cross-sectional transmission electron microscopy (TEM) observations clearly show that high-density dislocations (as indicated by red circles) are localized at the interface of the InAs and GaAs layers (**Figure 8**a).[26] Since the in-plane lattice constants gradually increase with increasing InAs thickness, it is likely that the density of misfit dislocations at the buried interface also increases during growth.[21]

As reported previously, we carried out X-ray diffraction (XRD) reciprocal-space map (RSM) measurements of the InAs on GaAs (111)A sample, and confirmed that nearly unstrained and

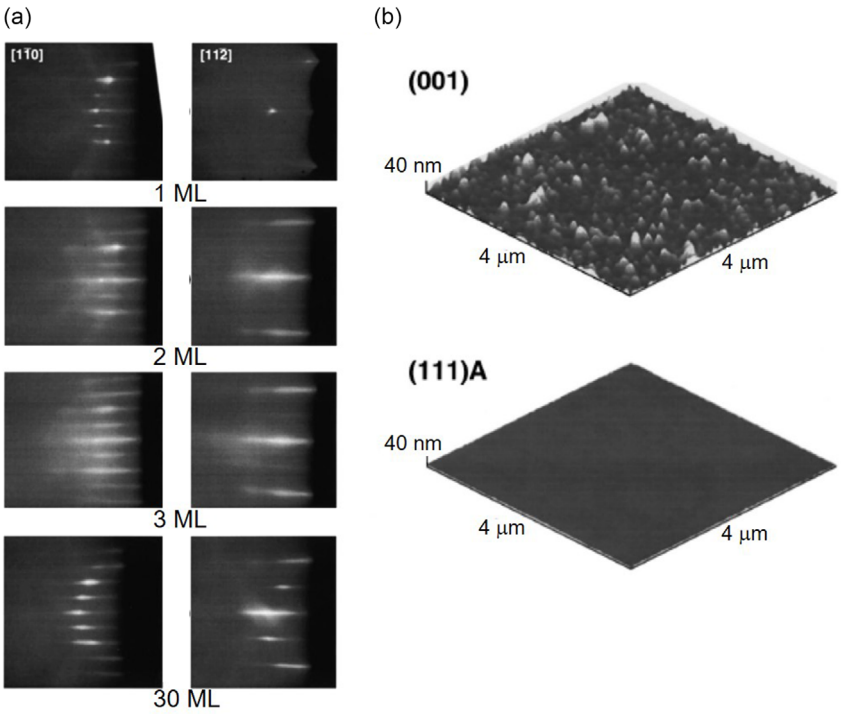

Figure 5. a) Evolution of the reflection high-energy electron diffraction (RHEED) pattern after the growth of InAs (1, 2, 3, and 30 ML [monolayer (ML)]) on GaAs (111)A. b) AFM images after growing 10 ML InAs on a) GaAs (001) and b) GaAs (111)A. The InAs was grown at 450 °C with a V/III ratio of 12. The growth rate was set at 0.5 ML s^{-1}. Reproduced with permission.[18] Copyright 1996, AIP Publishing.

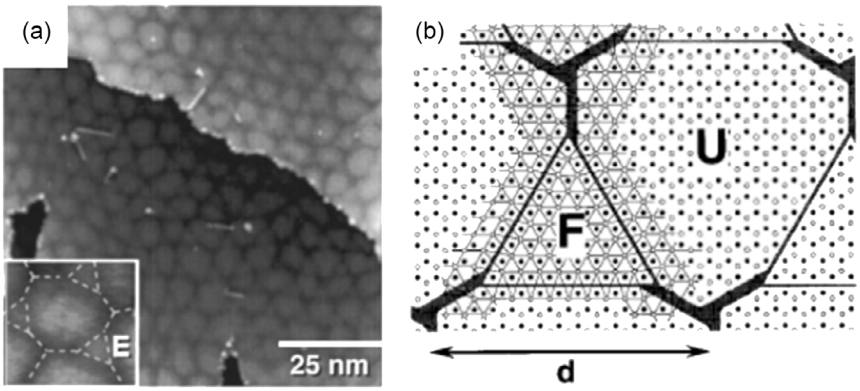

Figure 6. a) STM image of GaAs (111)A surfaces after the growth of 5 ML InAs. The InAs was grown at 450 °C with V/III ratio of 15. The growth rate was set at 0.077 ML s^{-1}. The STM image was obtained with sample voltages from −1.5 to −3.5 V, and tunneling currents of 0.08–0.2 nA. b) A model for the atomic structure at the InAs/GaAs (111)A interface. Reproduced with permission.[21] Copyright 1997, The American Physical Society.

uniform InAs layers are formed by introducing a misfit dislocation network at the interface.[23,26]

As discussed earlier, due to the unique lattice-relaxation mechanism of (111)A, most of the lattice relaxation takes place by formation of a dislocation network that is confined to the interface. If the formation of the dislocation network at the interface contributes to the reduction of threading dislocation (TD) density in the InAs layer, it is highly promising for the formation of high-quality metamorphic InAs layers. However, as shown in Figure 6, the misfit dislocation network is not perfect. Significant numbers of TDs (white spots) and SFs (white line segments) are visible in the STM image.[21] These defects propagate to the InAs surface and become visible in the plan-view TEM image (Figure 8b).[23,26] Typically, the surface densities of the TDs and SFs + SF tetrahedra are both around 10^9 cm^{-2}, as marked in Figure 8b.

Our systematic studies of the InAs/GaAs (111)A system have revealed another unique feature.[23] The X-ray rocking curve (XRC) of InAs grown on GaAs (111)A normally exhibits a very broad peak. As shown in **Figure 9**, the typical full width at half maximum of the InAs 111 reflection is more than 1500 arcsec for

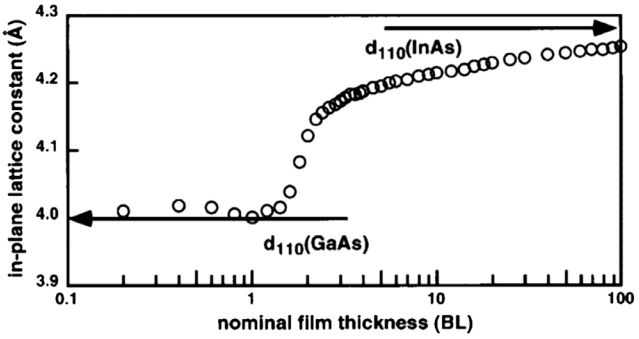

Figure 7. Change of in-plane lattice constant of the InAs layer on the GaAs (111)A substrates as a function of InAs thickness. The in-plane lattice constant (d_{110}) were measured from the distance between the 11 and $\overline{11}$ reflections in the RHEED patterns during the growth of InAs. The growth rate and III/V ratio were set at 0.01 ML s^{-1} and 50, respectively. Reproduced with permission.[22] Copyright 2000, The American Physical Society.

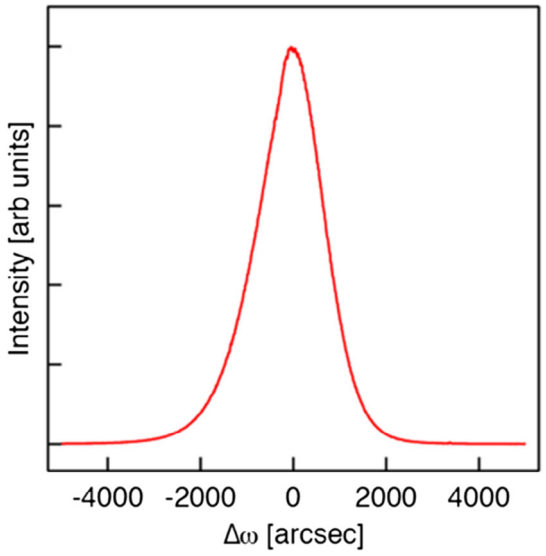

Figure 9. The 111 X-ray rocking curve of 100 nm InAs film grown on GaAs (111)A at 450 °C with an V/III flux ratio of ≈50. Reproduced under the terms of the CC-BY license.[23] Copyright 2020, Springer Nature.

100 nm InAs on GaAs (111)A. It is established that crystal imperfections cause a broadening of XRD profiles. Since the 115 reflection peak in the RSM is elongated in the direction perpendicular to the [115] azimuth, we attribute it to the misorientation of InAs lattice planes.[23]

As mentioned earlier, an unexpectedly high density of dislocations is formed in the InAs on GaAs (111)A. One may therefore conclude that InAs/GaAs (111)A metamorphic substrates are not suited for the fabrication of InAs-based devices, as the TDs will act as non-radiative recombination centers and channels for dark current in optoelectronic devices. While possible applications of InAs/GaAs (111)A have not been proposed, we have recently developed InAs-based infrared photodetectors based on the positive use of the InAs/GaAs (111)A interface.[26]

The detector structure consists of an *n*-InAs optical absorption layer directly grown with a thin undoped-GaAs spacer layer on *n*-GaAs, as shown in **Figure 10**. In this structure, we observed very low dark current density at a positive applied voltage (electrons flowing from *n*-GaAs to *n*-InAs) of up to ≈1 V at 77 K.[26] The Fermi level pinning effects caused by the misfit dislocation network at the interface significantly suppress the dark current even when we apply high voltage.[26,45–48] On irradiating with infrared light at 77 K, a clear photocurrent signal was observed; however, the details of the mechanism of photocurrent

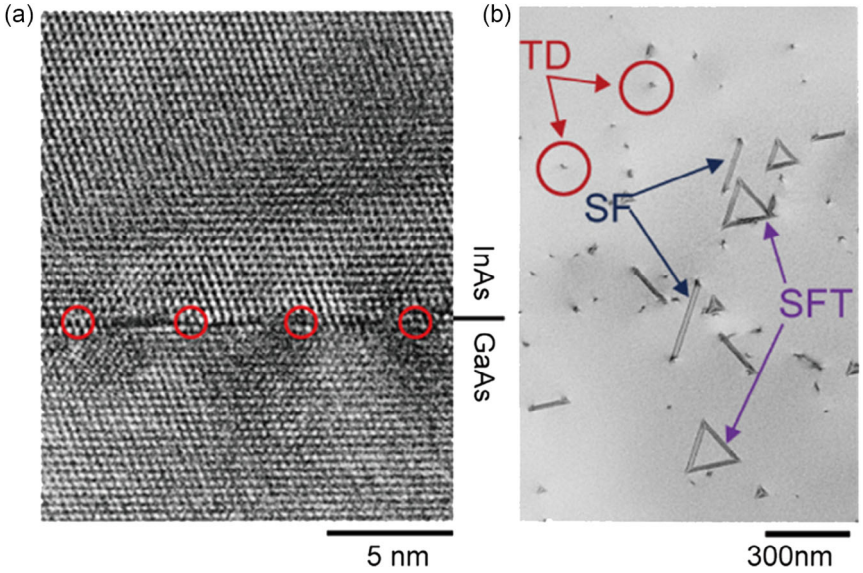

Figure 8. a) Cross-sectional and b) plan-view transmission electron microscopy (TEM) image of 300 nm InAs grown on GaAs (111)A at 460 °C. The growth rate for InAs and As_4 flux intensity were set at 1 ML s^{-1} and 3×10^{-5} Torr beam equivalent pressure, respectively. The red circles in (a) mark misfit dislocations at the interface; in (b), the threading dislocation (TD), stacking fault (SF), and stacking fault tetrahedron (SFT) are indicated by arrows. Reproduced with permission.[26] Copyright 2023, The American Chemical Society.

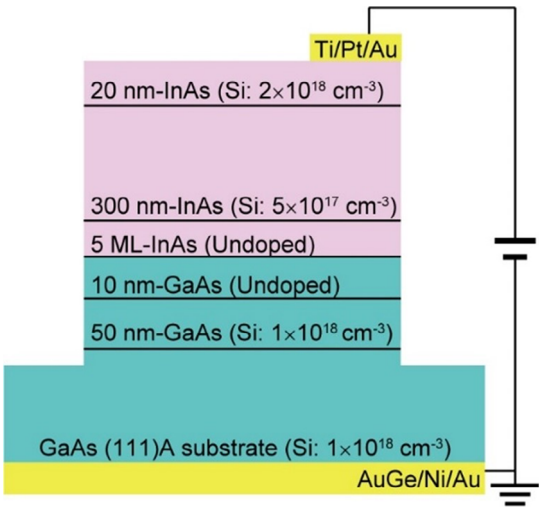

Figure 10. Schematic drawing of the InAs/GaAs (111)A photodetector structure. Reproduced with permission.[26] Copyright 2023, The American Chemical Society.

generation are still being studied. An interface with a high density of misfit dislocation is likely to play an important role in this phenomenon.[26,47,48] We also observed detector operation at 294 K with a 3.2 μm cutoff wavelength.[26] The detectivities at 77 and 294 K are reasonably good compared with commercialized InAs-based infrared (IR) detectors grown on InAs substrates, as shown in **Figure 11**.

3.2. Extension of the Growth of Lattice-Mismatched Layer on (111)A

When $In_xGa_{1-x}As$ ($x = 0.75$ or 0.5) or $In_xAl_{1-x}As$ ($x = 0.6$ or 0.52) is directly grown on GaAs (111)A, where lattice mismatch is

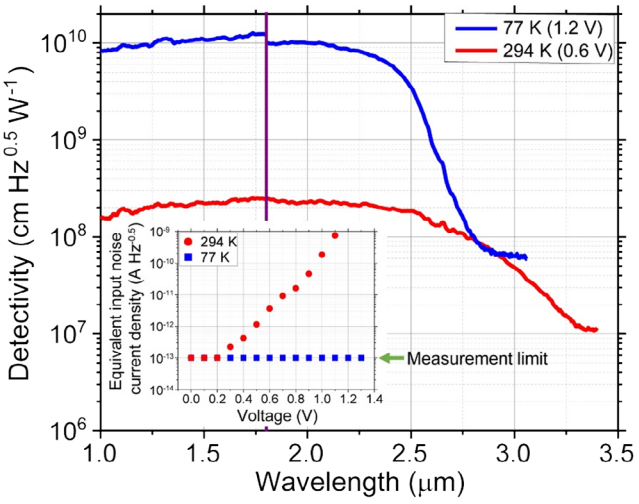

Figure 11. Detectivity spectra of the InAs/GaAs(111)A photodetector at 77 and 294 K with positive applied voltages of 1.2 and 0.6 V, respectively. The inset shows equivalent input noise current density (at 3 kHz) of the device at 77 and 294 K. Reproduced with permission.[26] Copyright 2023, The American Chemical Society.

3.2–5.4%, layer-by-layer growth also occurs and smooth surfaces are observed.[22,41] In the case of InAs on $In_xAl_{1-x}As$ ($x = 0.52$)/InP(111)A, where the lattice mismatch is around 3.2%, we have also observed layer-by-layer growth of InAs (Figure S1, Supporting Information).[24] In none of these cases was 3D island growth in SK growth mode observed. These results suggest that lattice mismatches at levels that exceed ≈3% cause the relaxation mechanism induced by the formation of the misfit dislocation network at the interface. In contrast, when $In_xGa_{1-x}As$ ($x = 0.25$) is grown on GaAs (111)A, where the lattice mismatch is less than 2%, the layer grows differently.[25] At the initial stage of the growth, strained InGaAs with smooth surface is grown. When the thickness exceed the critical thickness,[9–12] roughening of the surface is observed in AFM observation (**Figure 12**a). In Figure 12b, XRD–RSM around asymmetric 115 reflection, two peaks originating from the strained InGaAs (indicated by the red arrow) and from the relaxed InGaAs are clearly visible. These results clearly suggest that attempting strain relaxation by introducing an interface misfit dislocation network is not effective. To be able to grow relaxed layers whose lattice constant is close to the (111)A substrates, we have proposed the use of a thin InAs interlayer.[25] When InAs is grown on GaAs (111)A substrates, the in-plane lattice constant gradually changes from that of GaAs to InAs.[21,22] The in-plane lattice constant of InAs can therefore be adjusted to that of the InGaAs by controlling the thickness of InAs. Figure 12c shows AFM images of 150 nm $In_xGa_{1-x}As$ ($x = 0.25$) grown on 4.3 ML InAs/GaAs (111)A. A very smooth surface with a step-and-terrace structure is visible. The root-mean-square roughness is 0.57 nm. It is clear from the XRD–RSM image shown in Figure 12d that the peak originating from InGaAs is single and its position is very close to that of unstrained bulk InGaAs. Cross-sectional TEM observations show high-density misfit dislocations to be formed only at the InAs–GaAs interface and not at the InGaAs–InAs interface.[25] These results indicate that thin InAs acts as an effective buffer layer for relaxing the lattice mismatch by introducing a misfit dislocation network. More interestingly, we found that the thin InAs interlayer is elastically deformed by growing $In_xGa_{1-x}As$ on top together with the dislocation density change at the InAs/GaAs interface, even when the InAs thickness is not optimized: this approximates the concept of compliant substrates.[25,49] This flexibility, or immunity to experimental error, is highly promising for future applications.

It is thus possible to fabricate a virtual metamorphic substrate on GaAs (111)A with a desired lattice constant of $In_{1-x}Ga_xAs$ ($0 \leq x \leq 1$) using simple growth sequences.

Although we focus chiefly on the results of InAs growth on III–V semiconductor substrates in this review, the technique can be also applied to the growth of InAs on Si (111) substrates.[23,50,51] Techniques for growing III–V layers on Si substrates are highly important for research into Si photonics and/or electronic devices with III–V channel layers. Compared to the surface termination on Si (111) surfaces with In or As, we found that a smooth and lattice-relaxed InAs layer can be grown only on an In-terminated Si (111) surface.[50] Growth on As-terminated surfaces results in the formation of large 3D islands due to arsenic's surface passivation effect. The surface orientation of InAs grown on In-terminated surface is (111)A. Strain relaxation also occurs on introducing high-density misfit

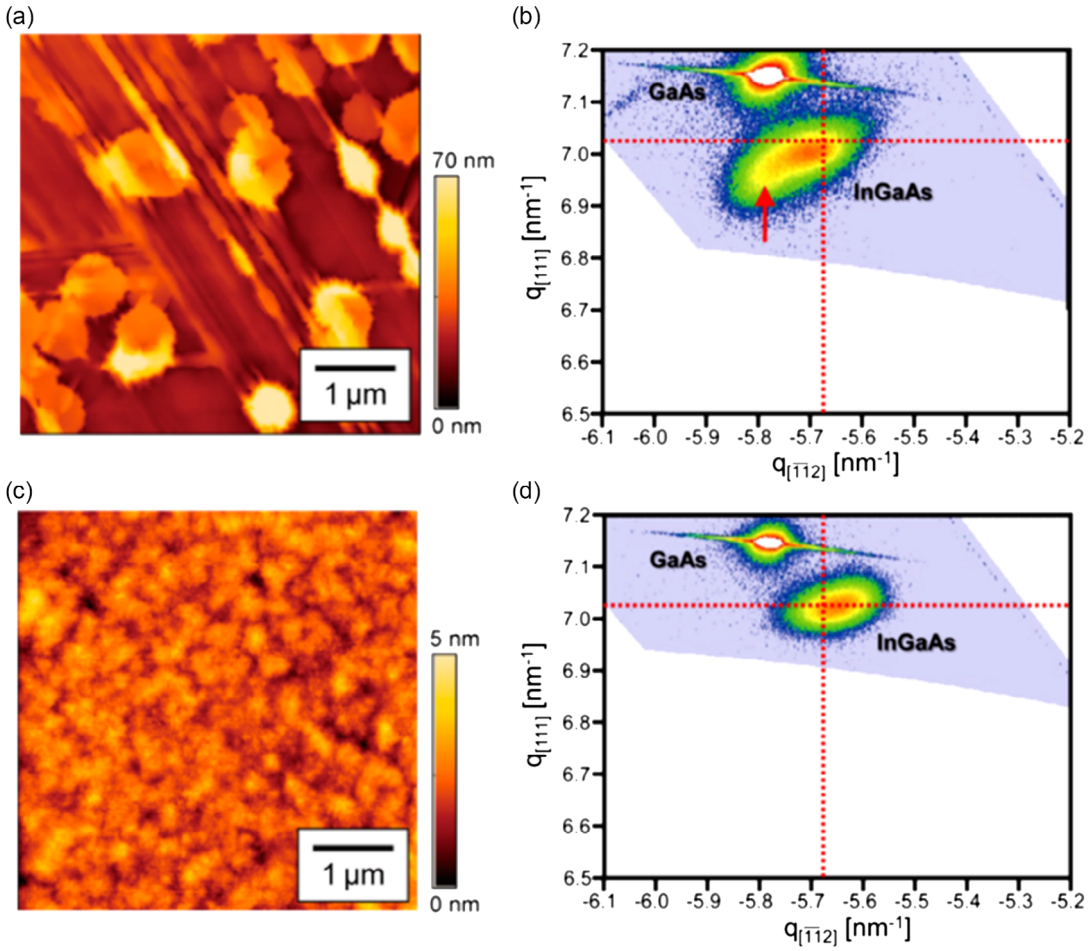

Figure 12. a,c) AFM image and b,d) X-ray diffraction reciprocal-space map (XRD–RSM) around asymmetric 115 reflection of 150 nm $In_{0.25}Ga_{0.75}As$ directly grown on GaAs (111)A (upper panel) and grown on 4.3 ML InAs interlayer/GaAs (111)A (lower panel). The InAs and InGaAs were grown at 450 °C with the growth rates of 0.085 and 0.3 ML s^{-1}, respectively. The As_4 flux intensity was set at 6–7 × 10^{-5} Torr beam equivalent pressure. Reproduced with permission.[25] Copyright 2016, The American Chemical Society.

dislocations at the interface, but the mechanism is slightly different from that of growth on GaAs (111)A. The InAs is nucleated with its inherent lattice constant from the beginning. No pseudomorphic InAs layer is formed, likely due to the excessive lattice mismatch of InAs/Si (11.5%).[23]

4. QD Growth on (111)A

In this section, we focus on the formation of elastically strained InAs QDs on lattice-mismatched (111)A substrates, in which a critical challenge is how to suppress dislocation formation. By using (111)A crystallographic surface with C_{3v} symmetry, formation of highly symmetrical InAs QDs can be expected. Single QDs with perfect in-plane symmetry can emit entangled photon pairs associated with cascade transition from the biexciton state to the ground state through the exciton state.[52] It is established that the widely studied InAs QDs grown on GaAs (001) substrates usually exhibit significant in-plane asymmetry due to the C_{2v} symmetry of the (001) surfaces.[53,54] InAs QD formation on (111)A with C_{3v} symmetry has been attempted to overcome this problem.[24,54] As discussed in the previous section, however, the SK mode is not applicable to the formation of InAs QDs on (111)A.[18] As an alternative approach, droplet epitaxy (DE) has been applied to the growth of InAs QDs. The fundamental idea of DE is based on the formation of liquid-metal droplets by a supply of group III atoms, followed by their crystallization into III–V semiconductor nanostructures, induced by a supply of group V atoms.[55–57] The DE of GaAs QDs/AlGaAs in lattice-matched systems has been intensively investigated over the last three decades.[38,56–58] High-quality entangled photon pair emission has been demonstrated.[38,59–62]

4.1. DE of InAs QDs on GaAs (111)A Substrates

First, InAs QDs growth on GaAs (111)A by DE was attempted, where lattice mismatch is 7.2%.[63] After the formation of In droplets on a GaAs (111)A substrate followed by crystallization into InAs with a supply of As_4 flux, InAs QDs are formed. Analysis of the RHEED pattern shows the QDs to be elastically strained and dislocation free at this stage. However, the

annealing of these QDs at a high temperature (450 °C) without capping causes lattice relaxation by introducing misfit dislocations.[63] The annealing of QDs without capping is an essential process in DE for the formation of high-quality QDs.[64,65] The density of QDs also decreases drastically due to the flattening (disappearing) of smaller QDs. Efficient light emission is unlikely from QDs with dislocations. As seen in Figure S2, Supporting Information, we have actually confirmed that no detectable photoluminescence (PL) emission was observed from capped InAs QDs. For conventional growth of InAs/GaAs with simultaneously supplied In and As molecules, as discussed in Section 3.1, a flat surface morphology and formation of misfit dislocations were more favored for growth on (111)A substrates than on (001) substrates. The present results therefore suggest that lattice mismatch of InAs/GaAs (7.2%) is too great to accommodate the elastic deformation of QDs on the (111)A substrate, even if 3D islands are formed by DE.

4.2. DE of InAs QDs on InP (111)A Substrates

To reduce the lattice mismatch between InAs and substrates, DE of InAs on InP (111)A has been investigated as a possible next step.[24] The lattice mismatch of InAs/InP is 3.2%. After droplet formation by a supply of In (0.8 or 1.6 ML) on $In_{0.52}Al_{0.48}As$/InP(111)A followed by crystallization using a supply of As_4 flux, InAs QDs form on the surfaces (**Figure 13**a,b). $In_{0.52}Al_{0.48}As$ is used at this point to create a lattice-matched buffer layer on the InP (111)A substrate. It is important to note that InAs QDs can be formed by a supply of In of less than 1 ML. There are no excess As atoms on the (111)A-(2 × 2) surfaces.[28] Nucleation of the In droplets therefore occurs immediately after supplying indium for droplet formation on the surface without forming a 2D layer, which is a characteristic feature when using (111)A substrates.[24,38,66] For droplet formation on (001)-c(4 × 4) surfaces, in contrast, 1.2–1.7 ML 2D layers are formed prior to droplet nucleation due to the presence of excess As atoms.[27,56,67]

Similar to the case of InAs QDs on GaAs(111)A, the uncapped annealing of the QDs at 370 °C causes significant reduction in QDs by flattening of small QDs in addition to the shrinkage of the large QDs, as seen in Figure 13c,d. The outflow of InAs from the QDs forms a 2D InAs layer around them.[24,68] Figure 13e shows a cross-sectional TEM image of a capped sample. The formation of a 1 ML thick 2D layer around the QDs is confirmed, as indicated by the arrow. Since no dislocation is visible around the QDs, it is clear that high-quality QDs without dislocation can be formed by using InP (111)A substrates.

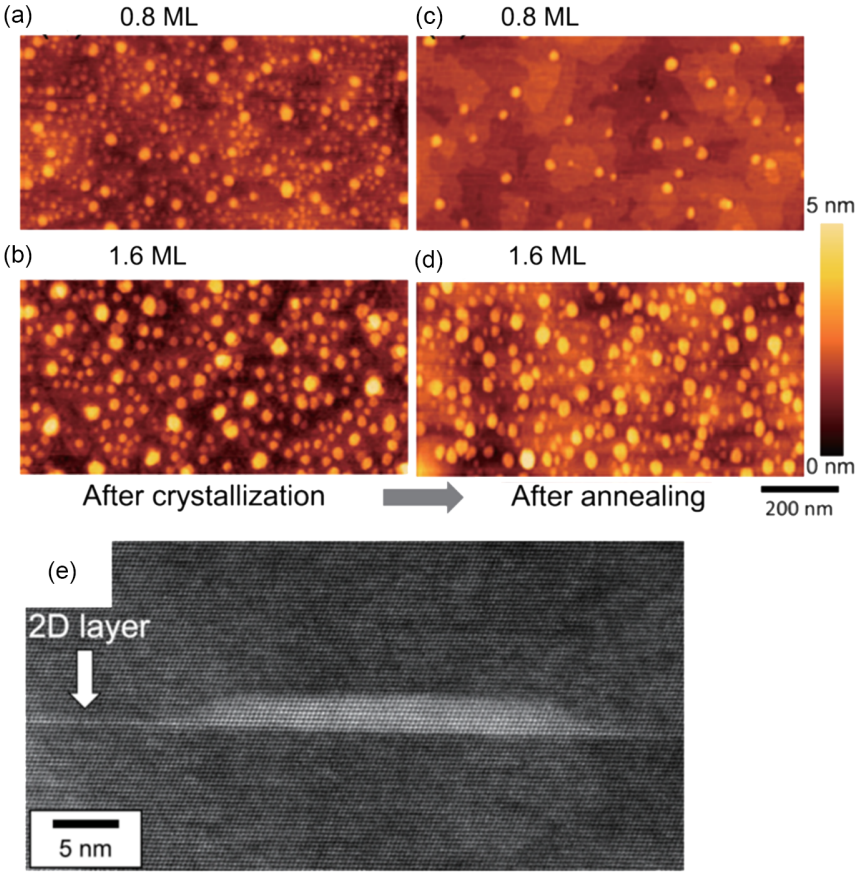

Figure 13. AFM images of a) 0.8 and b) 1.6 ML InAs quantum dots (QDs) on $In_{0.52}Al_{0.48}As$ after crystallization of the In droplets by a supply of As_4 flux (3×10^{-5} Torr beam equivalent pressure) at 270 °C. c,d) AFM images after annealing at 370 °C. e) Cross-sectional TEM image of 1.6 ML QDs after capping. The initial In droplets were formed at 270 °C by a supply of In flux without supply of As_4 flux. Reproduced with permission.[24] Copyright 2014, AIP Publishing.

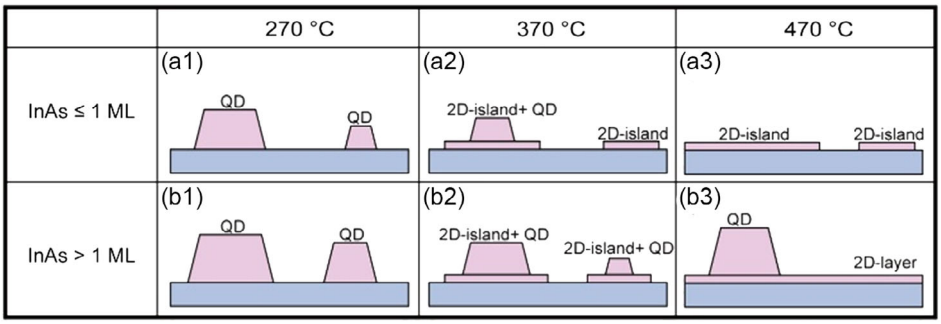

Figure 14. Schematic illustrations of structural evolution of InAs QDs after annealing. Reproduced with permission.[68] Copyright 2021, The American Chemical Society.

Systematic studies of DE of the InAs QDs on InAlAs/InP(111)A reveal a strain-induced QD formation mechanism after uncapped annealing,[68] as summarized in **Figure 14**. After annealing at 370 °C, the outflow of InAs from the QDs is suppressed after 2D InAs forms around the QDs to a certain limited extent (Figure 14a-2,b-2). Originally large QDs remain after annealing, while small QDs disappear and form 2D islands. In contrast, annealing at temperatures above 470 °C enhances the outflow of InAs from the QDs. The 2D growth continues until the entire surface is covered with a 1 ML thick 2D InAs layer. When the total amount of supplied InAs is greater than this saturation thickness (≈1 ML), QDs remain even after annealing (Figure 14b-3). However, no QDs remain after annealing with less than 1 ML InAs. The suppression of further 2D growth is attributable to minimizing the strain energy. As seen with SK growth, the total strain energy is reduced by retaining the InAs QDs + 2D InAs.[24,68] It is interesting that the order of formation of QDs and 2D InAs are reversed.

Figure 15 shows the PL spectra of InAs QDs capped by InAlAs.[24] The top panel was measured for the 0.8 ML QDs, and the bottom panel was measured for the 1.6 ML QDs. The emission spectra, which originate from the carrier recombinations in QDs, are observed to span from 950 to 1600 nm. Thus, the QDs are capable of emitting light within the O, C, and L telecommunications bands.[24,68,69] These very broad emission spectra are due to the wide distribution of QD sizes. The spectra consist of multiple split peaks, which are ascribed to the presence of different families of QDs whose heights vary in single-step ML increments.[24,38,53] The spectral split is consistent with the model calculations, in which we assumed a truncated QD shape with an atomically flat top, as shown in Figure 13e.[24] More remarkably, the PL signals are reliably observed even at 300 K thanks to the highly crystalline nature of these QD samples.[24]

The inset in the top panel of Figure 15 shows the low-temperature micro-PL spectrum of a single QD. It reveals a few split lines, which can be attributed to different exciton complexes. Later, we examined the polarization property of these single QDs and confirmed the formation of highly symmetrical QDs with nearly zero fine-structure splitting at telecommunication wavelengths.[70] More recently, we performed photon correlation and successfully observed anti-bunching characteristics, which constitute direct evidence of single-photon emission at a wavelength of around 1.55 μm.[70,71]

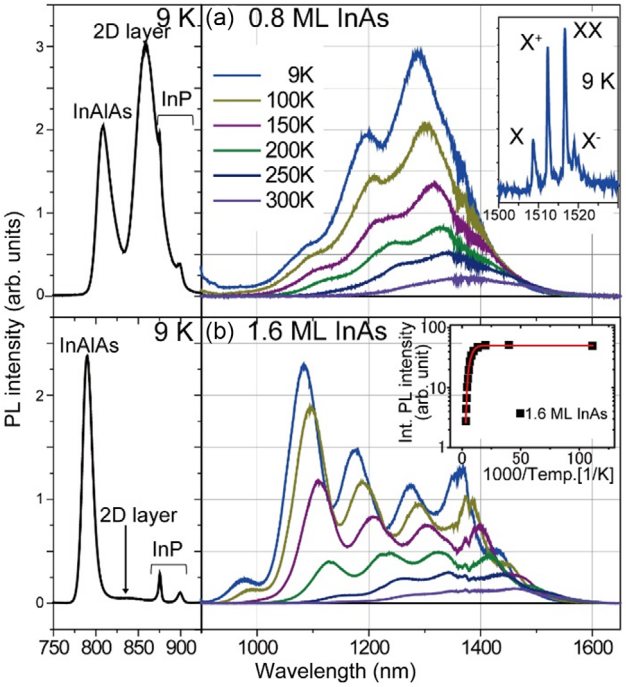

Figure 15. Photoluminescence (PL) spectra of a) 0.8 and b) 1.6 ML InAs QDs (right) on $In_{0.52}Al_{0.48}As$/InP(111)A at 9–300 K formed by droplet epitaxy (DE). PL spectra near 800 nm at 9 K (left) are also shown. The inset of (a) shows the μPL spectrum (at 9 K) of a single-InAs QD emitting at 1.5 μm. For the single-QD measurement, In droplets were formed by a supply of 0.4 ML In at 320 °C. The inset of (b) shows integrated PL intensity of 1.6 ML QDs as an inverse function of temperature. The red line corresponds to the fitting curve. Reproduced with permission.[24] Copyright 2014, AIP Publishing.

4.3. InAs QDs on Metamorphic InAlAs on GaAs (111)A Substrates

The integration of the technologies for lattice-relaxed layer formation (Section 3) and high-quality QD formation (Section 4) opens up another new possibility for quantum light-emitting devices. While highly luminescent InAs QDs can be formed on InP (111)A substrates, it is also highly desired to realize quantum light-emitting devices at telecommunications wavelengths

on GaAs substrates for practical applications. By using the strain-relaxation mechanism on GaAs (111)A, smooth $In_xAl_{1-x}As$ ($x = 0.52$ or 0.6), metamorphic buffer layers can be grown using relatively simple growth sequences.[68,72,73] The $In_{0.52}Al_{0.48}As$ was grown with insertion of thin InAs on precisely oriented GaAs (111)A[72] and the $In_{0.6}Al_{0.4}As$ was directly grown on vicinal GaAs (111)A (a miscut of 2° toward (1–12)).[42,73] Smooth InAlAs surfaces are observed in both cases. Using these metamorphic buffers as virtual substrates, InAs QDs are formed by DE. After capping, these InAs QDs show bright PL emission at around the telecommunication wavelengths of 1.3 and 1.55 μm, even at 300 K. While ensembles of the QDs exhibit bright PL signals, single isolated QDs frequently exhibit PL peaks with fairly broad linewidths. Polarization analysis also suggests that a majority of QDs suffer from serious optical anisotropy.[73] These drawbacks are likely attributable to the low quality of metamorphic InAlAs buffers. Further growth optimization is therefore necessary.

5. Conclusion

In this article, we reviewed heteroepitaxial growth of InAs on lattice-mismatched (111)A substrates. On GaAs (111)A substrates, a misfit dislocation network is formed at the initial stage of InAs growth and 3D island growth by the SK mode is inhibited. The lattice mismatch between the InAs and GaAs is gradually relaxed during growth of 1.5–5 ML InAs and the lattice-relaxed InAs layer is continuously grown in layer-by-layer mode. While flat surfaces are formed, the formation of a high density of TDs and a broad XRC are confirmed. These are challenges that remain to be solved. It has been confirmed that the relaxation mechanism by the formation of a misfit dislocation network at the interface takes place for $In_xGa_{1-x}As$ ($x > 0.5$) and $In_yAl_{1-y}As$ ($x > 0.5$) on GaAs (111)A, InAs/InP (111)A, and InAs/Si (111), in which the lattice mismatch is large. However, this mechanism does not work with $In_xGa_{1-x}As$ ($x = 0.25$)/GaAs (111)A. We have found that the insertion of a thin InAs interlayer effectively relaxes the lattice mismatch. The InAs interlayer is elastically deformed by growing $In_xGa_{1-x}As$ on top together with a dislocation density change at the InAs/GaAs interface. Possible applications of the InAs/GaAs(111) structure have recently been proposed. By taking advantage of the InAs/GaAs interface with high-density misfit dislocations, we have demonstrated a new type of infrared photodetector. Due to the strong band pinning effect, low dark current operation is realized in the shortwave infrared range.

We also show the formation of highly luminescent InAs QDs without dislocation on InAlAs/InP (111)A substrates. Since SK growth cannot be used in this system, we have applied DE. The systematic studies revealed that 2D InAs layers are formed by the flow of InAs from the QDs during the uncapped annealing. The final structure of QDs + a 2D layer is similar to that achieved in SK mode, but the order of formation is reversed. High-yield PL emission at around telecommunication wavelengths was observed in macro- and micro-PL. The integration of lattice-relaxed layer formation and high-quality QDs formation to create highly luminescent QDs can be realized on GaAs (111)A substrates by using metamorphic InAlAs buffers.

By elucidating and controlling the characteristic strain-relaxation mechanism on (111)A substrates, new possibilities have been opened for InAs-based photonic devices.

Supporting Information

Supporting Information is available from the Wiley Online Library or from the author.

Acknowledgements

The authors would like to express sincere thanks to Drs. H. T. Miyazaki, T. Kawazu, M. Jo, T. Noda, N. Ha, Y. Sakuma, K. Mitsuishi, and K. Sakoda, National Institute for Materials Science, Dr. A. Castellano and Prof. S. Sanguinetti, University of Milano-Bicocca, Profs. B. Urbaszek, X. Marie, and T. Amand, Université de Toulouse. This work was supported by grant no. JPJ004596 from the Innovative Science and Technology Initiative for Security, ATLA, Japan.

Conflict of Interest

The authors declare no conflict of interest.

Keywords

(111)A, dislocation, heteroepitaxy, InAs, quantum dots

Received: October 2, 2023
Revised: November 29, 2023
Published online: December 12, 2023

[1] E. Yablonovitch, E. Kane, *J. Lightwave Technol.* **1986**, *4*, 504.
[2] A. R. Adams, *Electron. Lett.* **1986**, *22*, 249.
[3] F. C. Frank, J. H. van der Merwe, *Proc. R. Soc. London, Ser. A* **1949**, *198*, 205.
[4] L. Goldstein, F. Glas, J. Y. Mazin, M. N. Charasse, G. L. Roux, *Appl. Phys. Lett.* **1985**, *47*, 1099.
[5] D. Leonard, M. Krishnamurthy, C. M. Reaves, S. P. Denbaars, P. M. Petroff, *Appl. Phys. Lett.* **1993**, *63*, 3203.
[6] Y. Nabetani, T. Ishikawa, S. Noda, A. Sasaki, *J. Appl. Phys.* **1994**, *76*, 347.
[7] Y. Arakawa, H. Sakaki, *Appl. Phys. Lett.* **1982**, *40*, 939.
[8] N. Kirstaedter, N. N. Ledentsov, M. Grundmann, D. Bimberg, V. M. Ustinov, S. S. Ruvimov, M. V. Maximov, P. S. Kop'ev, Zh. I. Alferov, U. Richter, P. Werner, U. Gösele, J. Heydenreich, *Electron. Lett.* **1994**, *30*, 1416.
[9] J. W. Matthews, A. E. Blakeslee, *J. Cryst. Growth* **1974**, *27*, 118.
[10] J. W. Matthews, A. E. Blakeslee, *J. Cryst. Growth* **1975**, *29*, 273.
[11] J. W. Matthews, A. E. Blakeslee, *J. Cryst. Growth* **1976**, *32*, 265.
[12] R. People, J. C. Bean, *Appl. Phys. Lett.* **1985**, *47*, 322.
[13] I. García, J. F. Geisz, R. M. France, J. Kang, S.-H. Wei, M. Ochoa, D. J. Friedman, *J. Appl. Phys.* **2014**, *116*, 074508.
[14] T. Kujofsa, J. E. Ayers, *J. Vac. Sci. Technol. B* **2014**, *32*, 031205.
[15] Z. Y. Zhang, A. E. H. Oehler, B. Resan, S. Kurmulis, K. J. Zhou, Q. Wang, M. Mangold, T. Süedmeyer, U. Keller, K. J. Weingarten, R. A. Hogg, *Sci. Rep.* **2012**, *2*, 477.

[16] B.-D. Liu, R.-M. Lin, S.-C. Lee, T.-P. Sun, *J. Vac. Sci. Technol., B* **1997**, *15*, 321.
[17] I. Shibasaki, *J. Cryst. Growth* **1997**, *175/176*, 13.
[18] H. Yamaguchi, M. R. Fahy, B. A. Joyce, *Appl. Phys. Lett.* **1996**, *69*, 776.
[19] K. Kanisawa, Y. Yamaguchi, Y. Hirayama, *Appl. Phys. Lett.* **2000**, *76*, 589.
[20] H. Yamaguchi, J. L. Sudijono, B. A. Joyce, T. S. Jones, C. Gatzke, R. A. Stradling, *Phy. Rev. B* **1998**, *58*, R4219.
[21] H. Yamaguchi, J. G. Belk, X. M. Zhang, J. L. Sudijono, M. R. Fahy, T. S. Jones, D. W. Pashley, B. A. Joyce, *Phy. Rev. B* **1997**, *55*, 1337.
[22] A. Ohtake, M. Ozeki, J. Nakamura, *Phy. Rev. Lett.* **2000**, *84*, 4665.
[23] A. Ohtake, T. Mano, Y. Sakuma, *Sci. Rep.* **2020**, *10*, 4606.
[24] N. Ha, X. Liu, T. Mano, T. Kuroda, K. Mitsuishi, A. Castellano, S. Sanguinetti, T. Noda, Y. Sakuma, K. Sakoda, *Appl. Phys. Lett.* **2014**, *104*, 143106.
[25] T. Mano, K. Mitsuishi, N. Ha, A. Ohtake, A. Castellano, S. Sanguinetti, T. Noda, Y. Sakuma, T. Kuroda, K. Sakoda, *Cryst. Growth Des.* **2016**, *16*, 5412.
[26] T. Mano, A. Ohtake, T. Kawazu, H. T. Miyazaki, Y. Sakuma, *ACS Appl. Mater. Interfaces* **2023**, *15*, 29636.
[27] A. Ohtake, *Surf. Sci. Rep.* **2008**, *63*, 295.
[28] S. Y. Tong, G. Xu, W. N. Mei, *Phy. Rev. Lett.* **1984**, *52*, 1693.
[29] K. W. Haberern, M. D. Pashley, *Phy. Rev. B* **1990**, *41*, 3226.
[30] J. M. C. Thornton, P. Welghtman, D. A. Woolf, C. J. Dunscombe, *Phy. Rev. B* **1995**, *51*, 14459.
[31] A. Ohtake, J. Nakamura, T. Komura, T. Hanada, T. Yao, H. Kuramochi, M. Ozeki, *Phy. Rev. B* **2001**, *64*, 045318.
[32] A. Ohtake, T. Akiyama, T. Ito, *Surf. Sci.* **2012**, *606*, 1864.
[33] K. Sato, M. R. Fahy, B. A. Joyce, *Surf. Sci.* **1994**, *315*, 105.
[34] M. Nishizawa, T. Eguchi, S. Omoto, T. Osaka, *Appl. Surf. Sci.* **1997**, *121*, 204.
[35] C. H. Li, Y. Sun, D. C. Law, S. B. Visbeck, R. F. Hicks, *Phys. Rev. B* **2003**, *68*, 085320.
[36] A. Taguchi, K. Kanisawa, *Appl. Surf. Sci.* **2006**, *252*, 5263.
[37] K. D. Vallejo, T. A. Garrett, K. E. Sautter, K. Saythavy, B. Liang, P. J. Simmonds, *J. Vac. Sci. Technol., B* **2019**, *37*, 061810.
[38] T. Mano, M. Abbarchi, T. Kuroda, B. McSkimming, A. Ohtake, K. Mitsuishi, K. Sakoda, *Appl. Phys. Express* **2010**, *3*, 065203.
[39] T. Uehara, T. Iwai, I. Yoshiba, Y. Horikoshi, *Jpn. J. Appl. Phys.* **2007**, *46*, 496.
[40] C. D. Yerino, B. Liang, D. Huffaker, P. J. Simmonds, M. L. Lee, *J. Vac. Sci. Technol. B* **2017**, *35*, 010801.
[41] L. Esposito, S. Bietti, A. Fedorov, R. Nötzel, S. Sanguinetti, *Phy. Rev. Mat.* **2017**, *1*, 024602.
[42] A. Tuktamyshev, S. Vichi, F. Cesura, A. Fedorov, S. Bietti, D. Chrastina, S. Tsukamoto, S. Sanguinetti, *J. Cryst. Growth* **2022**, *600*, 126906.
[43] A. Barbiero, A. Tuktamyshev, G. Pirard, J. Huwer, T. Müller, R. M. Stevenson, S. Bietti, S. Vichi, A. Fedorov, G. Bester, S. Sanguinetti, A. J. Shields, *Phys. Rev. Appl.* **2022**, *18*, 034081.
[44] A. M. Hassanen, J. Herranz, L. Geelhaar, R. B. Lewis, *Semicond. Sci. Technol.* **2023**, *38*, 095009.
[45] H. Yamaguchi, Y. Hirayama, *J. Cryst. Growth* **1999**, *201/202*, 778.
[46] T. Kawazu, T. Mano, Y. Sakuma, *Jpn. J. Appl. Phys.* **2023**, *62*, 074001.
[47] M. Lampert, *Phys. Rev.* **1956**, *103*, 1648.
[48] W. G. Oldham, A. G. Milnes, *Solid-State Electron.* **1964**, *7*, 153.
[49] C. Carter-Coman, R. Bicknell-Tassius, A. S. Brown, N. M. Jokerst, *Appl. Phys. Lett.* **1997**, *70*, 1754.
[50] A. Ohtake, K. Mitsuishi, *J. Vac. Sci. Technol. B* **2011**, *29*, 031804.
[51] A. Ohtake, T. Mano, N. Miyata, T. Mori, T. Yasuda, *Appl. Phys. Lett.* **2014**, *104*, 032101.
[52] O. Benson, C. Santori, M. Pelton, Y. Yamamoto, *Phys. Rev. Lett.* **2000**, *84*, 2513.
[53] R. Seguin, A. Schliwa, S. Rodt, K. Pötschke, U. W. Pohl, D. Bimberg, *Phys. Rev. Lett.* **2005**, *95*, 257402.
[54] A. Schiliwa, M. Winkelnkemper, A. Lochmann, E. Stock, D. Bimberg, *Phys. Rev. B* **2009**, *80*, 161307(R).
[55] N. Koguchi, S. Takahashi, T. Chikyow, *J. Cryst. Growth* **1991**, *111*, 688.
[56] K. Watanabe, N. Koguchi, Y. Gotoh, *Jpn. J. Appl. Phys.* **2000**, *39*, L79.
[57] M. Gurioli, Z. Wang, A. Rastelli, T. Kuroda, S. Sanguinetti, *Nat. Mat.* **2019**, *18*, 799.
[58] M. Abbarchi, C. A. Mastrandrea, T. Kuroda, T. Mano, K. Sakoda, N. Koguchi, S. Sanguinetti, A. Vinattieri, M. Gurioli, *Phys. Rev. B* **2008**, *78*, 125321.
[59] T. Kuroda, T. Mano, N. Ha, H. Nakajima, H. Kumano, B. Urbaszek, M. Jo, M. Abbarchi, Y. Sakuma, K. Sakoda, I. Suemune, X. Marie, T. Amand, *Phys. Rev. B.* **2013**, *88*, 041306(R).
[60] M. Jo, T. Mano, M. Abbarchi, T. Kuroda, Y. Sakuma, K. Sakoda, *Cryst. Growth Des.* **2012**, *12*, 1411.
[61] N. Ha, T. Mano, T. Kuroda, Y. Sakuma, K. Sakoda, *Appl. Phys. Lett.* **2019**, *115*, 083106.
[62] F. B. Basset, S. Bietti, M. Reindl, L. Esposito, A. Fedorov, D. Huber, A. Rastelli, E. Bonera, R. Trotta, S. Sanguinetti, *Nano Lett.* **2018**, *18*, 505.
[63] S. Bietti, L. Esposito, A. Fedorov, A. Ballabio, A. Martinelli, S. Sanguinetti, *Nanoscale Res. Lett.* **2015**, *10*, 247.
[64] T. Mano, M. Abbarchi, T. Kuroda, C. A. Mastrandrea, A. Vinattieri, S. Sanguinetti, K. Sakoda, M. Gurioli, *Nanotechnology* **2009**, *20*, 395601.
[65] M. Jo, G. Duan, T. Mano, K. Sakoda, *Nanoscale Res. Lett.* **2011**, *6*, 76.
[66] A. Ohtake, N. Ha, T. Mano, *Cryst. Growth. Des.* **2015**, *15*, 485.
[67] T. Mano, T. Kuroda, K. Mitsuishi, M. Yamagiwa, X.-J. Guo, K. Furuya, K. Sakoda, N. Koguchi, *J. Cryst. Growth* **2007**, *301–302*, 740.
[68] T. Mano, A. Ohtake, N. Ha, T. Noda, Y. Sakuma, T. Kuroda, K. Sakoda, *Cryst. Growth Des.* **2021**, *21*, 3947.
[69] N. Ha, T. Mano, Y.-N. Wu, Y.-W. Ou, S.-J. Chen, Y. Sakuma, K. Sakoda, T. Kuroda, *Appl. Phys. Express* **2016**, *9*, 101201.
[70] X. Liu, N. Ha, H. Nakajima, T. Mano, T. Kuroda, B. Urbaszek, H. Kumano, I. Suemune, Y. Sakuma, K. Sakoda, *Phys. Rev. B* **2014**, *90*, 081301(R).
[71] N. Ha, T. Mano, S. Dubos, T. Kuroda, Y. Sakuma, K. Sakoda, *Appl. Phys. Express* **2020**, *13*, 025002.
[72] N. Ha, T. Mano, T. Kuroda, K. Mitsuishi, A. Ohtake, A. Castellano, S. Sanguinetti, T. Noda, Y. Sakuma, K. Sakoda, *Jpn. J. Appl. Phys.* **2015**, *54*, 04DH07.
[73] A. Tuktamyshev, A. Fedorov, S. Bietti, S. Vichi, K. D. Zeuner, K. D. Jöns, D. Chrastina, S. Tsukamoto, V. Zwiller, M. Gurioli, S. Sanguinetti, *Appl. Phys. Lett.* **2021**, *118*, 133102.

Takaaki Mano is a group leader of the Semiconductor Epitaxial Structure Group at National Institute for Materials Science (NIMS). He received his doctorate from the University of Tokyo in 2001. From 2001 to 2003, he was resident at COBRA Inter-University Research Institute, Eindhoven University of Technology, in the Netherlands, as a postdoc researcher. In 2004, he moved to NIMS. His current research interests are crystal growth and characterization of III–V-based semiconductor heterostructures by molecular-beam epitaxy with a special interest in their application to novel optical devices.

Akihiro Ohtake received his doctorate from Waseda University in 1996. He joined Joint Research Center for Atom Technology (JRCAT) in 1996, and moved to National Institute for Materials Science (NIMS) in 2001. He has been working on the epitaxial growth of III–V semiconductors and transition-metal dichalcogenides using molecular-beam epitaxy and structural analysis of their surface reconstructions.

Takashi Kuroda is a chief researcher/group leader of the Quantum Photonics Group at the Research Center for Electronic and Optical Materials within National Institute for Materials Science (NIMS). He completed his B.Sc. (1990), M.Sc. (1992), and Ph.D. (1994) in physics at Hokkaido University. After working for the Tokyo Institute of Technology as a research associate (1995–2003), he joined NIMS as a senior researcher (2004). He also has the position of adjunct professor at Kyushu University. His current research interests include semiconductor optics and spectroscopy, the physics of quantum dots and 2D materials, and the application of nanophotonics to mid-infrared lasers.